steady and constant probe tuning, and therefore highly accurate pulses, are essential. As noted already, the two-quantum line shapes that we obtained did not provide us with any additional information with which to identify adsorbed species.

Conclusions

NMR spectroscopic techniques have allowed direct quantitative observation of coordinatively adsorbed ammonia, NH_4^+ ions, a decomposed species assigned to NH_2, and surface hydroxyls. The observed distribution of these species as a function of adsorption temperature and catalyst compositions suggests the following scheme for the adsorption and decomposition of ammonia on these catalysts:

$$Ti + NH_3(g) \rightarrow H_3N{>}Ti \quad \text{(low loadings)} \quad (2a)$$

$$V{=}O + NH_3(g) \rightarrow H_3N{>}V{=}O \quad \text{(low loadings)} \quad (2b)$$

$$2V{=}O + NH_3(g) \rightarrow VOH + NH_2(s) \quad \text{(higher loadings)} \quad (3a)$$

$$2VOH \rightarrow V{=}O + V^{III,IV} + H_2O(g) \quad \text{(higher loadings)} \quad (3b)$$

$$V^{III,IV} + NH_2(s) \rightarrow V^{III,IV}NH_2 \quad \text{(higher loadings)} \quad (3c)$$

$$VOH + NH_3(g) \rightarrow VO{-}NH_4^+ \quad \text{(fast, all loadings)} \quad (4)$$

$$V^{III,IV}NH_2 \rightarrow V^{III,IV} + N_s + H_2O(g) \quad \text{(higher loadings)} \quad (5)$$

Reactions 2a and 2b represent the coordinative adsorption of ammonia to the Lewis acid sites of the vanadia and the titania. Reaction 3a represents the decomposition of NH_3 on the higher weight loading samples. Reaction 4, the formation of ammonium ions, is a fast reaction that occurs on all vanadia-containing samples where surface hydroxyls are present, but in greater proportion on the higher weight loading samples where the ammonia decomposition makes available additional hydroxyl groups. Reactions 3b and 3c represent the dehydration and reduction of the surface and most likely account for the low-temperature water desorption peak that is concomitant with the ammonia desorption (reaction 4) on the higher weight loading samples, as well as the reduction of vanadium atoms to the +3 or +4 state. Reaction 5 is the formation of surface N atoms that can lead to N_2 or other dissociated nitrogen products; it also represents additional water formation from the decomposed ammonia and could explain the second high-temperature water peak in the TPD[18] of the 3.0 and 6.1 wt % samples, which coincides with the evolution of nitrogen products.

If extrapolation of the observations of adsorbed ammonia to conditions where NO_x and oxygen are also present is possible, it is surmised that ammonium ions are not responsible for the majority of the catalytic activity, as they are easily removed by heating to temperatures below those where the activity reaches a maximum. In addition, observation of rapidly rotating ammonia, under all conditions where intact ammonia is observed, strongly suggests that any long-lived activated complex involving adsorbed ammonia fixed to more than one site on the surface (i.e. H-bonded to several neighboring oxygen atoms) in unlikely. These results put an upper limit on the lifetime of such species (as has been proposed in the Eley-Rideal mechanism[2,38,39]) of about one measured rotational period of the adsorbed ammonia, which is no greater than ~ 10 μs at room temperature.

The results presented here and elsewhere suggest that dissociative adsorption of ammonia occurs predominantly on polymeric vanadia species where surface VO bonds are in close proximity to one another and results in increased activity but decreased selectivity toward nitrogen in the selective catalytic reduction reaction. Indeed, reduced sites are also found to be active for the SCR mechanism.[3] A coordinated NH_2NO species reacting to form $N_2 + H_2O$, as proposed on the basis of mass spectrometric studies,[40] may be a key intermediate.

Acknowledgment. We wish to acknowledge technical discussions with Professor Alexis T. Bell and his research group. We also wish to thank Heather Rumsey for assistance with the sample preparation and surface area measurements and Phil Armstrong for assistance with the deuteron NMR experiments. This work was supported by the Director, Office of Energy Research, Office of Basic Energy Sciences, Materials Sciences Division of the U.S. Department of Energy, under Contract DEACO3-76SF00098.

Registry No. V_2O_5, 1314-62-1; TiO_2, 13463-67-7; ammonia, 7664-41-7.

Glass Formation and Structure in Non-Oxide Chalcogenide Systems. The Short Range Order of Ag_2S-P_2S_5 Glasses Studied by ^{31}P MAS-NMR and Dipolar NMR Techniques

Zhengming Zhang, John H. Kennedy, and Hellmut Eckert*

Contribution from the Department of Chemistry, University of California, Santa Barbara, California 93106. *Received January 13, 1992*

Abstract: Glass formation and the local structure of ionically conductive crystalline and glassy compositions in the $(Ag_2S)_x(P_2S_5)_{1-x}$ system have been investigated by ^{31}P magic-angle spinning (MAS) and spin-echo NMR. Glass formation encompasses the compositional range $0.5 \leq x \leq 0.67$. ^{31}P MAS and spin-echo NMR data reveal striking differences in the local structure of the glasses and their crystalline counterparts. This result reinforces previous findings in related pseudobinary chalcogenide systems. A detailed examination of the Ag_2S-P_2S_5 phase diagram reveals seven stable crystalline pseudobinary compounds with stoichiometries $AgPS_3$, $Ag_4P_2S_6$ (two crystallographic modifications), $Ag_4P_2S_7$, $Ag_7P_3S_{11}$, Ag_3PS_4, and Ag_7PS_6, respectively, plus an additional compound with yet uncertain stoichiometry. The ^{31}P-^{31}P dipole-dipole coupling present in P-P and P-S-P connectivities in these phases has been characterized by means of spin-diffusion measurements under MAS conditions. This technique appears particularly useful in the compositional and structural analysis of multicomponent phase mixtures as they arise from the crystallization of glasses.

Introduction

The discovery of very high ionic conductivity in a new class of sulfide-based glasses has been one of the most significant developments in the field of solid electrolytes in the past few years.[1-13] These glasses form by rapid quenching of melts containing Li_2S, LiI, and stoichiometric group III-V sulfides, such as B_2S_3, SiS_2,

(1) Malugani, J. P.; Robert, G. *Solid State Ionics* **1980**, *1*, 519.

0002-7863/92/1514-5775$03.00/0

Table I. Synthesis Conditions of the Samples Studied $[(Ag_2S)_x(P_2S_5)_{1-x}$ and $Ag_4P_2S_6$-I and -II] and Identified Phases (from X-ray Powder Diffraction and Solid-State NMR)

samples	experimental conditions	identified phases
x =		
0.20	750 °C melt, 300 °C 1 day	$AgPS_3$, P_4S_{10}, P_4S_9
0.25	750 °C melt, 300 °C 1 day	$AgPS_3$, P_4S_{10}, P_4S_9
0.33	850 °C melt, 300 °C 1 day	$AgPS_3$, P_4S_{10}, P_4S_9
0.33	850 °C melt, 800 °C quench	glass (169)[a] + P_4S_9
0.40	850 °C melt, 300 °C 1 day	$AgPS_3$, P_4S_{10}, P_4S_9
0.40	850 °C melt, 800 °C quench	glass (176)[a] + P_4S_9
0.50	850 °C melt, 500 °C 1 day	$AgPS_3$
0.50	850 °C melt, 800 °C quench	glass (192)[a]
0.60	850 °C melt, 500 °C 1 day	$Ag_4P_2S_7$, $AgPS_3$
0.60	850 °C melt, 500 °C 1 day	new phase ($Ag_4P_2S_7$, $AgPS_3$)
0.60	850 °C melt, 800 °C quench	glass (212)[a]
0.67	550 °C solid state, 6 days	$Ag_4P_2S_7$ ($Ag_7P_3S_{11}$)
0.67	850 °C melt, 800 °C quench	glass (221)[a]
$Ag_4P_2S_6$-I	850 °C melt, 550 °C 2 days (20% excess P and S)	$Ag_4P_2S_6$-I ($AgPS_3$)
$Ag_4P_2S_6$-II	850 °C melt, 550 °C 2 days	$Ag_4P_2S_6$-II
x =		
0.70	850 °C melt, 550 °C 1 day	$Ag_7P_3S_{11}$
0.70	850 °C melt, 800 °C quench	glass + Ag_3PS_4
0.75	850 °C, 600 °C 1 day	Ag_3PS_4 (new phase)
0.80	850 °C melt, 600 °C 1 day	Ag_7PS_6 + Ag_3PS_4
0.875	900 °C melt, 600 °C 1 day	Ag_7PS_6

[a] Glass-transition temperature (°C) listed in parentheses.

and P_2S_5. Considerable experimental work has been undertaken to maximize conductivity and chemical stability of these compounds. It has been more recently that, driven by the search for structural guidelines to optimize materials properties, the microstructure of these glasses has moved into the focus of attention.[14-18] As previously shown, solid-state NMR is an element-selective, inherently-quantitative method ideally suited for structural studies of glasses. For example, ^{31}P MAS-NMR has proven immensely successful for elucidating the local phosphorus environments in alkali phosphate glasses and corresponding crystalline phases.[19-27] Unique chemical shift ranges have been assigned to orthophosphate ($Q^{(0)}$), pyrophosphate ($Q^{(1)}$), and metaphosphate ($Q^{(2)}$) species. The compositional dependence of their occurrences is in quantitative agreement with the continuous network modification model. This model states that upon introduction of alkaline oxide into P_2O_5 each oxide ion reacts with a P–O–P bridge resulting in the formation of two new non-bridging oxygen atoms.[28]

Recent studies in our laboratory have explored whether and to what extent similar structural principles hold in the stoichiometrically analogous sulfide systems. These studies, which initially focused on ionically conductive lithium sulfide-based systems, revealed dramatic differences in the short-range order between the crystalline and the glassy state.[29,30] It is of interest whether such behavior is general to pseudobinary non-oxide chalcogenide glasses that include other cations. In the present contribution we report, for the first time, the preparation of glasses in the system Ag_2S–P_2S_5 and their structural characterization by systematic solid-state NMR studies. Furthermore, we will characterize the known crystalline compounds in this system by MAS, spin–echo, and spin–diffusion measurements and discuss these spectral features in relationship to published single-crystal X-ray data. This information will then be used to interpret corresponding solid-state NMR experiments on Ag_2S–P_2S_5 glasses in terms of structural models.

Experimental Section

Sample Preparation and Characterization. Tables I and II give an overview of the samples investigated, the conditions of their preparation, glass-transition temperatures, and NMR parameters. Since the starting and resultant materials are extremely hygroscopic and air sensitive, all sample manipulations were carried out under a helium atmosphere with H_2O level less than 2 ppm. $(Ag_2S)_x(P_2S_5)_{1-x}$ glasses were synthesized within evacuated quartz ampules from commercial Ag_2S (99.9%) and P_2S_5 (99%). While commercial P_2S_5 is known to contain a mixture of P_4S_{10}, P_4S_9, and S_8,[31] these components are expected to equilibrate under the reaction conditions. The samples were heated at 800–900 °C for 0.5 h and then quenched from ca. 800 °C in ice water. The glassy character was verified by X-ray powder diffraction (Scintag diffractometer). Glass transition temperatures were measured on a DuPont 912 differential scanning calorimeter, using a heating rate of 10 °C/min. All samples within the compositional range $0.67 \geq x \geq 0.5$ show single transitions (followed by recrystallization exotherms), indicating the formation of homogeneous glasses. The quenched $x = 0.33$ and 0.4 compositions appear entirely amorphous according to X-ray diffraction, but they show two glass transition temperatures, suggesting phase separation. Furthermore, the solid-state NMR spectra show small amounts of crystalline impurities, identified with reference to literature data[32,33] as P_4S_9 and P_4S_{10}. Table I reveals that with increasing x, the T_g values increase monotonically. This behavior parallels that previously found for Li_2S–P_2S_5 glasses[30] and contrasts that typically seen for other network former-network modifier systems, including oxide glasses. The trend observed in these systems with increasing lithium or silver sulfide content reflects the monotonic change from the molecularly organized P_2S_5 glass to a material held together more and more strongly by coulombic forces.

A number of crystalline model compounds and variable mixed compositions were synthesized according to the procedures listed in Table I. The products were characterized by X-ray powder diffraction and solid-state NMR. To ensure the reproducibility of the results, replicate samples were studied for most compositions.

NMR Studies. Nuclear magnetic resonance studies were carried out on a General Electric GN-300 widebore system, equipped with a multinuclear magic-angle spinning probe from DOTY Scientific. For chemical shift tensor evaluations, the samples were spun within sapphire

(2) Robert, G.; Malugani, J. P.; Saida, A. *Solid State Ionics* **1981**, *3/4*, 311.
(3) Malugani, J. P.; Fahys, B.; Mercier, R.; Robert, G.; Duchange, J. P.; Baudry, S.; Broussely, M.; Gabano, J. P. *Solid State Ionics* **1983**, *9/10*, 659.
(4) Mercier, E.; Malugani, J. P.; Fahys, B.; Robert, G. *Solid State Ionics* **1981**, *5*, 663.
(5) Duchange, J. P.; Malugani, J. P.; Fahys, B.; Robert, G. *Prog. Batteries Sol. Cells* **1981**, *4*, 46.
(6) Ribes, M.; Barrau, B.; Souquet, J. L. *J. Noncryst. Solids* **1980**, *38/39*, 271.
(7) Wada, H.; Menetrier, M.; Levasseur, A.; Hagenmuller, P. *Mater. Res. Bull.* **1983**, *18*, 189.
(8) Pradel, A.; Ribes, M. *Solid State Ionics* **1986**, *18/19*, 351.
(9) Kennedy, J.; Yang, Y. *J. Solid State Chem.* **1987**, *69*, 252.
(10) Zhang, Z.; Kennedy, J. H. *Solid State Ionics* **1990**, *38*, 217.
(11) Sahami, S.; Shea, S. W.; Kennedy, J. H. *J. Electrochem. Soc.* **1985**, *132*, 985.
(12) Kennedy, J. H.; Sahami, S.; Shea, S. W.; Zhang, Z. *Solid State Ionics* **1986**, *18/19*, 368.
(13) Kennedy, J. H.; Zhang, Z.; Eckert, H. *J. Noncryst. Solids* **1990**, *123*, 328.
(14) Dembovskii, S. A.; Chechetkina, E. A. *J. Noncryst. Solids* **1986**, *85*, 346.
(15) Bicerano, J.; Ovshinsky, S. R. *J. Noncryst. Solids* **1985**, *74*, 75.
(16) Boolchand, P. *Hyperfine Interact.* **1986**, *27*, 3.
(17) Phillips, J. C. *J. Noncryst. Solids* **1979**, *34*, 153.
(18) Phillips, J. C. *J. Noncryst. Solids* **1981**, *43*, 37.
(19) Turner, G. L.; Smith, K. A.; Kirkpatrick, R. J.; Oldfield, E. *J. Magn. Reson.* **1986**, *70*, 408.
(20) Villa, M.; Scagliotti, M.; Chiodelli, G. *J. Noncryst. Solids* **1987**, *94*, 101.
(21) Brow, R.; Kirkpatrick, R.; Turner, G. *J. Noncryst. Solids* **1990**, *116*, 39.
(22) Hayashi, S.; Hayamizu, K. *J. Solid State Chem.* **1989**, *80*, 195.
(23) Villa, M.; Carduner, K. R.; Chiodelli, G. *J. Solid State Chem.* **1987**, *69*, 19.
(24) Grimmer, A. R.; Wolf, G. U. *Eur. J. Solid State Inorg. Chem.* **1991**, *28*, 221.
(25) Prabhakar, S.; Rao, K. J.; Rao, C. N. R. *Chem. Phys. Lett.* **1987**, *139*, 96.
(26) Duncan, T. M.; Douglass, D. C. *Chem. Phys.* **1984**, *87*, 339.
(27) Griffiths, L.; Root, A.; Harris, R. K.; Packer, K. J.; Chippendale, A. M.; Tromans, F. R. *J. Chem. Soc., Dalton Trans.* **1986**, 2247.
(28) Van Wazer, J. R. *J. Am. Chem. Soc.* **1950**, *72*, 644.
(29) Eckert, H. *Angew. Chem.* **1989**, *101*, 1763.
(30) Eckert, H.; Zhang, Zh.; Kennedy, J. H. *Chem. Mater.* **1990**, *2*, 273.
(31) Demarq, M. C. *Phosphorus Sulfur* **1981**, *11*, 65.
(32) Eckert, H.; Liang, C. S.; Stucky, G. D. *J. Phys. Chem.* **1989**, *93*, 452.
(33) Harris, R. K.; Wilkes, P. J.; Wood, P. T.; Woollins, J. D. *J. Chem. Soc., Dalton Trans.* **1989**, 805.

Table II. NMR Parameters of Glassy and Crystalline Phases in the System $Ag_2S-P_2S_5$

crystalline compds	δ_{iso} (±0.1 ppm)	δ_{11} (±5 ppm)	δ_{22} (±5 ppm)	δ_{33} (±5 ppm)	$M_2(^{31}P)^c$ (10^6 rad^2 s^{-2})	k^e [s^{-1}]
$AgPS_3$	64.4	−139	135	197	9.8 (6.7)	
$Ag_4P_2S_6$-I	114.9[a]					0.032
	98.6[a]					
$Ag_4P_2S_6$-II	125.3[b] (a)		not determined			a–b: 0.030
	111.2[b] (b)					a–c: 0.002
	103.1 (c)	89	105	115		b–c: 0.003
unknown	91.5	43	97	135		
$Ag_4P_2S_7$	96.5	55	98	137	3.2 (2.4)	
$Ag_7P_3S_{11}$	103.3 (a)	87	105	117	2.1 (2.0)	a–b: 0.040
	101.1 (b)	51	114	139		a–c: 0.010
	91.9 (c)	54	85	137		b–c: 0.018
Ag_3PS_4	103.0	89	105	115	1.2	
Ag_7PS_6	101.7	97	101	107	0.6	
glasses $(Ag_2S)_x(P_2S_5)_{1-x}$						
$x = 0.33$[d]	87/97				5.6	
$x = 0.40$[d]	86/98				5.3	
$x = 0.50$	86/97				5.1	
$x = 0.60$	85/98				3.6	
$x = 0.67$	98				2.8	

[a] $^1J(^{31}P-^{31}P)$ = 109 Hz. [b] $^1J(^{31}P-^{31}P)$ = 109 Hz. [c] Estimated error ±10%; calculated values in parentheses. [d] Impurities of crystalline P_4S_9, P_4S_{10}. [e] Average from both inversion experiments, estimated error ±10%.

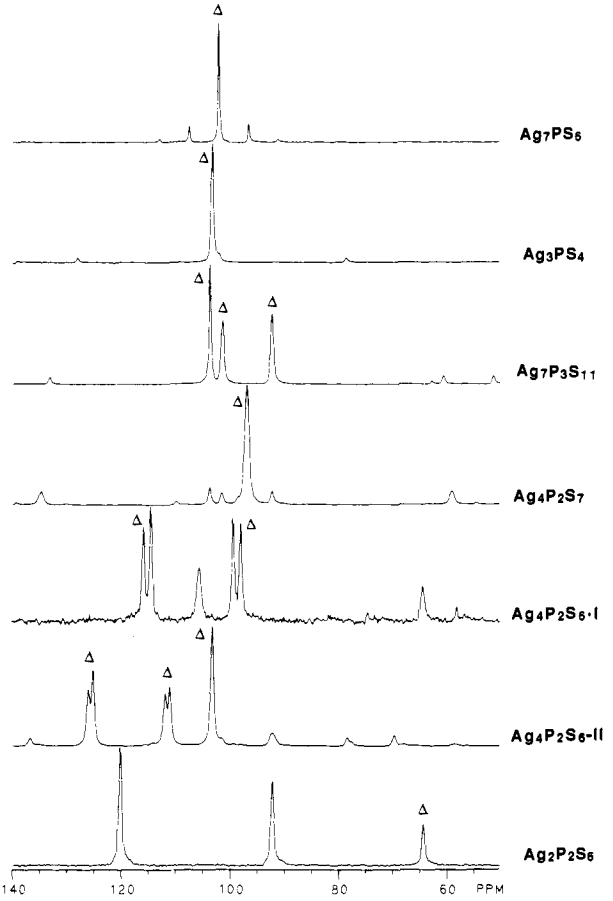

Figure 1. 121.65-MHz ^{31}P MAS-NMR spectra of the known crystalline silver phosphorus sulfides. The triangular symbol identifies the centerbands. Minor, unlabeled peaks arise from spinning sidebands of the compound studied and/or from central and spinning sidebands of impurity phases.

or silicon nitride spinners of 7 mm o.d. at variable speeds between 0.24 and 8 kHz. Spin-diffusion measurements (see below) were carried out at a closely controlled fixed spinning speed of 5.000 ± 0.002 kHz and at reduced power (90° pulse of 18 μs length). All the other experiments were conducted at maximum power available with 90° pulses of 5–6 μs length. Recycle delays were varied between 1 min and 10 h to ensure spectra free from saturation effects. Typical delays were 0.2–1 h for the glassy and 1–3 h for the crystalline samples. To avoid hydrolysis by atmospheric moisture, the spinners were sealed with a thin layer of high-vacuum grease.

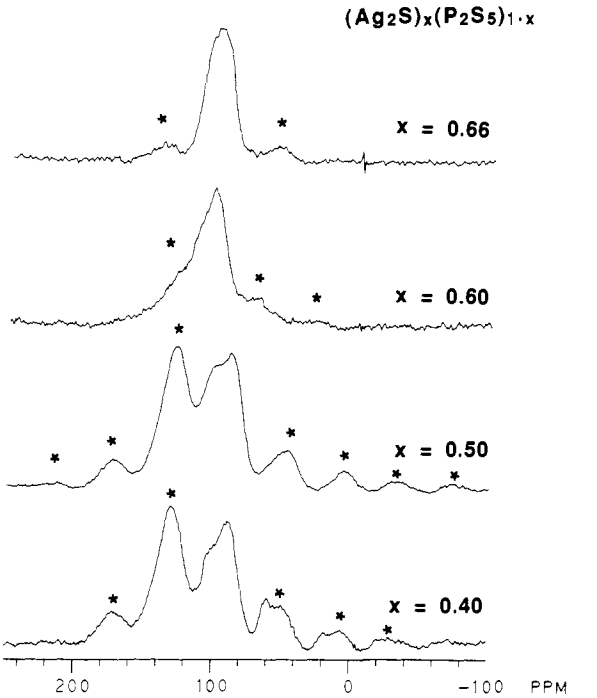

Figure 2. 121.65-MHz ^{31}P MAS spectra of glasses in the system $(Ag_2S)_x(P_2S_5)_{1-x}$. x values are indicated. Spinning sidebands are indicated by asterisks.

Results and Data Analysis

Chemical Shift Spectroscopy. Previous studies have shown the existence of the following pseudobinary compounds in the system $Ag_2S-P_2S_5$: $AgPS_3$,[34] two modifications of $Ag_4P_2S_6$,[35-37] $Ag_4P_2S_7$,[38] $Ag_7P_3S_{11}$,[39] Ag_3PS_4[40] and Ag_7PS_6.[41] With the exception

(34) Toffoli, P.; Khodadad, P.; Rodier, N. *Acta Crystallogr.* **1978**, *B34*, 3561.
(35) Toffoli, P.; Khodadad, P.; Rodier, N. *Acta Crystallogr.* **1983**, *C39*, 1485.
(36) Toffoli, P.; Michelet, A.; Khodadad, P.; Rodier, N. *Acta Crystallogr.* **1982**, *B38*, 706.
(37) Toffoli, P.; Khodadad, P. *C. R. Seances Acad. Sci. Paris* **1980**, *291*, 275.
(38) Toffoli, P.; Khodadad, P.; Rodier, N. *Acta Crystallogr.* **1977**, *B33*, 1492.
(39) Toffoli, P.; Khodadad, P.; Rodier, N. *Acta Crystallogr.* **1982**, *B38*, 2374.
(40) Andrae, H.; Blachnik, R. *J. Therm. Anal.* **1989**, *35*, 595.

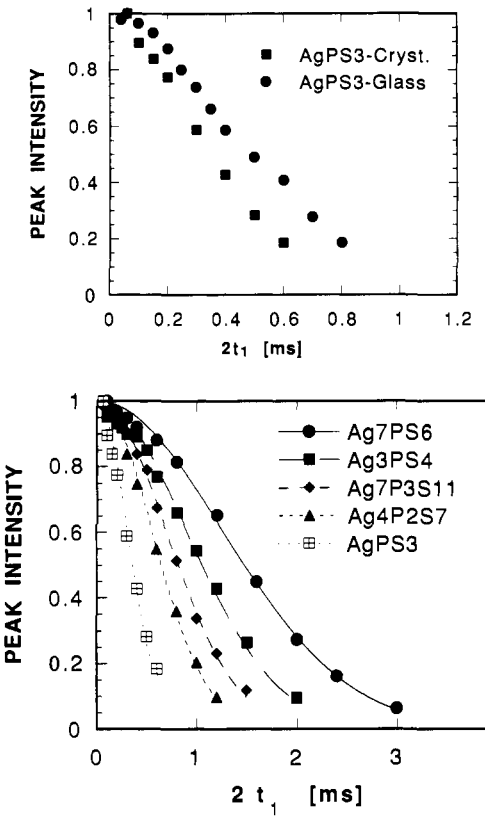

Figure 3. 121.65-MHz spin-echo decays for glasses and crystalline compounds in the system Ag_2S–P_2S_5: (a, top) $x = 0.5$; comparison of glassy and crystalline material. (b, bottom) Spin-echo decays for the crystalline compounds. The various curves are guides to the eye.

of the last two compounds, their structures have been solved by single-crystal X-ray diffraction. Figure 1 shows the ^{31}P MAS-NMR spectra of the known crystalline silver phosphorus sulfides. These spectra can be compared with those obtained for the glasses, shown in Figure 2. Table II summarizes the chemical shift information obtained from these spectra. Isotropic chemical shifts are externally referenced to 85% H_3PO_4. Chemical shift anisotropies are estimated from the spinning sideband intensities, using the graphical procedure of Herzfeld and Berger.[42] These results are reported with downfield shifts positive and the convention $\delta_{33} > \delta_{22} > \delta_{11}$.

Dipolar Spin-Echo NMR. In both the glasses and relevant crystalline materials, the ^{31}P–^{31}P dipole–dipole coupling was characterized by static ^{31}P spin-echo experiments. These studies were carried out using a 90°–t_1–180° pulse sequence as previously described.[43,44] Typical data are summarized in Figure 3. With increasing evolution time $2t_1$, the spin-echo intensities $I(2t_1)$ decrease in an approximately Gaussian fashion, as theoretically expected from the expression

$$I(2t_1)/I(0) = \exp[-\{(2t_1)^2 M_{2d}/2\}]$$

From these decays, second moments M_{2d} characterizing the homodipolar ^{31}P–^{31}P coupling were extracted. Figure 4 summarizes the compositional dependence of these values for the crystalline and glassy samples under investigation. Due to the rigorous distance dependence of the dipole–dipole coupling strength, these M_{2d} values possess direct structural significance. For any structure, theoretical M_{2d}'s can be calculated from the internuclear distances, using the van Vleck formulae.[45] Thus,

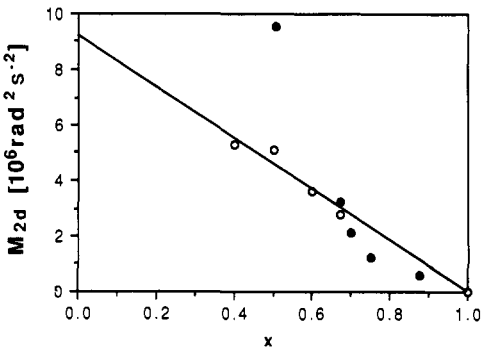

Figure 4. Compositional dependence of the ^{31}P–^{31}P dipolar second moment M_{2d} (see text) as a function of x for the crystalline (filled circles) and glassy (open circles) samples under investigation. The solid curve is a linear least-squares fit to the glass data.

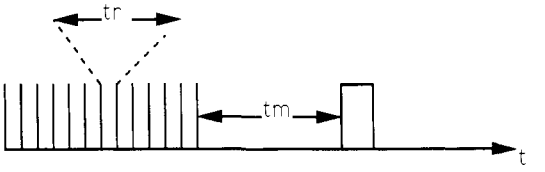

Figure 5. Pulse sequence for measuring spectral spin diffusion with MAS. In the present experiments, the selective 180° pulse is composed of fifteen 12° pulses (2.4 μs length), and the spinning speed is 5.000 ± 0.002 kHz. This corresponds to a pulse spacing of 200 μs in the DANTE sequence. The mixing period t_m is incremented systematically, with t_m values ranging from 10 ms to 600 s in the present application.

Table II compares the experimental and calculated second moments for the crystalline model compounds studied here.

Spin-Diffusion Measurements. Spin diffusion is a term used to describe the exchange of longitudinal (z) magnetization among the various constituents of a (generally) homonuclear spin system. This process, which is mediated by either dipolar or scalar spin–spin coupling, requires that the total Zeeman energy is conserved. Hence one might (erroneously) conclude that the nuclei involved must have identical (or indistinguishable) resonance frequencies for spin diffusion to occur. Rather, "spectral" spin diffusion can also be observed between inequivalent spins that have widely different resonance frequencies if there is a mechanism that balances any mismatch in the Zeeman energies. In many cases, such conditions are given when the two interacting spins under consideration also interact with a strongly coupled heteronuclear spin system (usually protons).[46–50] A different example for such a balancing mechanism is the rotational resonance effect, where the dipolar coupling between two spins is re-introduced by setting the sample rotation rate equal to the chemical shift difference.[51–53] In the present application, neither mechanism is at work. Rather, spectral spin diffusion due to MAS is a consequence of the fact that for each spin the resonance frequency changes over the rotor period along a characteristic trajectory depending on crystal orientation. Spin diffusion will then occur during the rotor cycle, whenever the corresponding trajectories of two coupled spins intersect or approach each other within a frequency difference comparable to the strength of the internuclear dipole–dipole coupling.[47] The probability of this "level crossing" will generally depend on a large number of variables such as the following: the crystal orientation, the relative orientation of the chemical shift

(41) Toffoli, P.; Khodadad, P. *C. R. Seances Acad. Sci. Paris* **1978**, *286*, 349.
(42) Herzfeld, J.; Berger, A. E. *J. Chem. Phys.* **1980**, *73*, 6021.
(43) Lathrop, D.; Eckert, H. *J. Am. Chem. Soc.* **1989**, *111*, 3536. Lathrop, D.; Eckert, H. *Phys. Rev. B* **1991**, *43*, 7279.
(44) Franke, D.; Maxwell, R.; Lathrop, D.; Eckert, H. *J. Am. Chem. Soc.* **1991**, *113*, 4822.
(45) Van Vleck, J. H. *Phys. Rev.* **1948**, *74*, 1168.
(46) Kubo, A.; McDowell, C. A. *J. Chem. Phys.* **1988**, *89*, 63.
(47) Kubo, A.; McDowell, C. A. *J. Chem. Soc., Faraday Trans.* **1988**, *84*, 3713.
(48) Vanderhart, D. L. *J. Magn. Reson.* **1987**, *72*, 13.
(49) Suter, D.; Ernst, R. R. *Phys. Rev. B* **1985**, *32*, 5068.
(50) Henrichs, P. M.; Linder, M.; Hewitt, J. M. *J. Chem. Phys.* **1986**, *85*, 7077.
(51) Andrew, E. R.; Bradbury, A.; Eades, R. G.; Wynn, V. T. *Phys. Lett.* **1963**, *4*, 99.
(52) Andrew, E. R.; Clough, S.; Farnell, L. F.; Glendhill, T. D.; Roberts, I. *Phys. Lett.* **1966**, *5*, 505.
(53) Raleigh, D. P.; Levitt, M. H.; Griffin, R. G. *Chem. Phys. Lett.* **1988**, *146*, 71.

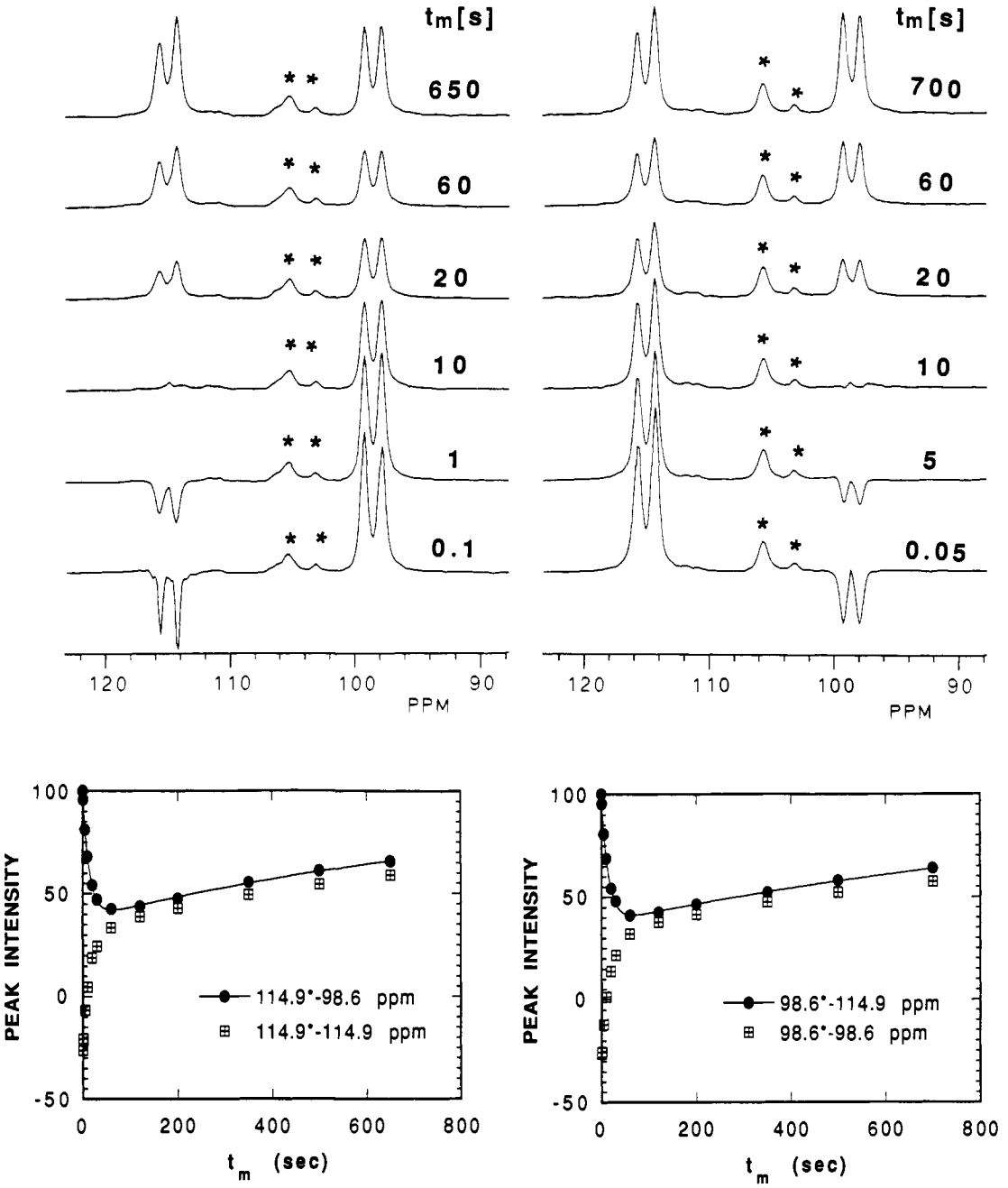

Figure 6. Spectral spin-diffusion experiments on $Ag_4P_2S_6$-I. Shown at the top of the figure are selected spectra as a function of t_m. Impurity phases that are not affected by the pulse sequence are labeled with an asterisk. The dependence of signal intensity (percent relative to the unperturbed state) on mixing time is shown at the lower part of the figure. The chemical shifts of the inverted peak (labeled with an asterisk) and of the monitored peak are indicated.

tensors for the two nuclei involved, and the strength of the internuclear interaction, as well as the rotation frequency.

Experimentally, spectral spin diffusion in solids has been monitored by selective saturation or inversion of one resonance and then monitoring the effect on the intensities of the other, unperturbed resonances.[46-49,54,55] Our experiments were conducted with the pulse sequence shown in Figure 5, previously developed and applied to doped fluoroapatites by Yesinowski and coworkers.[56] This sequence uses a rotor-synchronized DANTE pulse train[57] to invert selectively a chosen resonance with its associated spinning sidebands. During the mixing period t_m, ^{31}P–^{31}P dipole–dipole or scalar coupling effects cross-relaxation between spatially close or bonded phosphorus nuclei, resulting in a change of spin state populations. The concomitant changes in the magnetization are then monitored by a nonselective 90° read pulse at the end of the mixing period t_m. Figures 6–8 show typical results obtained for the two $Ag_4P_2S_6$ phases and for $Ag_7P_3S_{11}$. The signal intensities seen are affected both by site-to-site cross-relaxation and spin–lattice relaxation. Both of these processes can generally be assumed to follow first-order kinetics. The phenomenological analysis adopted here, details of which will be published elsewhere,[58] parametrizes the observed changes in signal intensity during t_m in terms of a single cross-relaxation rate constant k and a spin–lattice relaxation time T_1. It is important to bear in mind, however, that in reality the number k only represents a "grand average" of widely different values for different crystal orientations.

(54) Caravatti, P.; Levitt, M. H.; Ernst, R. R. *J. Magn. Reson.* **1986**, *68*, 323.
(55) Bork, V.; Schaefer, J. *J. Magn. Reson.* **1989**, *81*, 196.
(56) Moran, L. B.; Berkowitz, J. K.; Yesinowski, J. P. *Phys. Rev. B* **1992**, *45*, 5347.
(57) Bodenhausen, G.; Freeman, R.; Morris, G. A. *J. Magn. Reson.* **1976**, *23*, 171.

(58) Zhang, Z.; Kennedy, J. H.; Eckert, H. Submitted for publication.

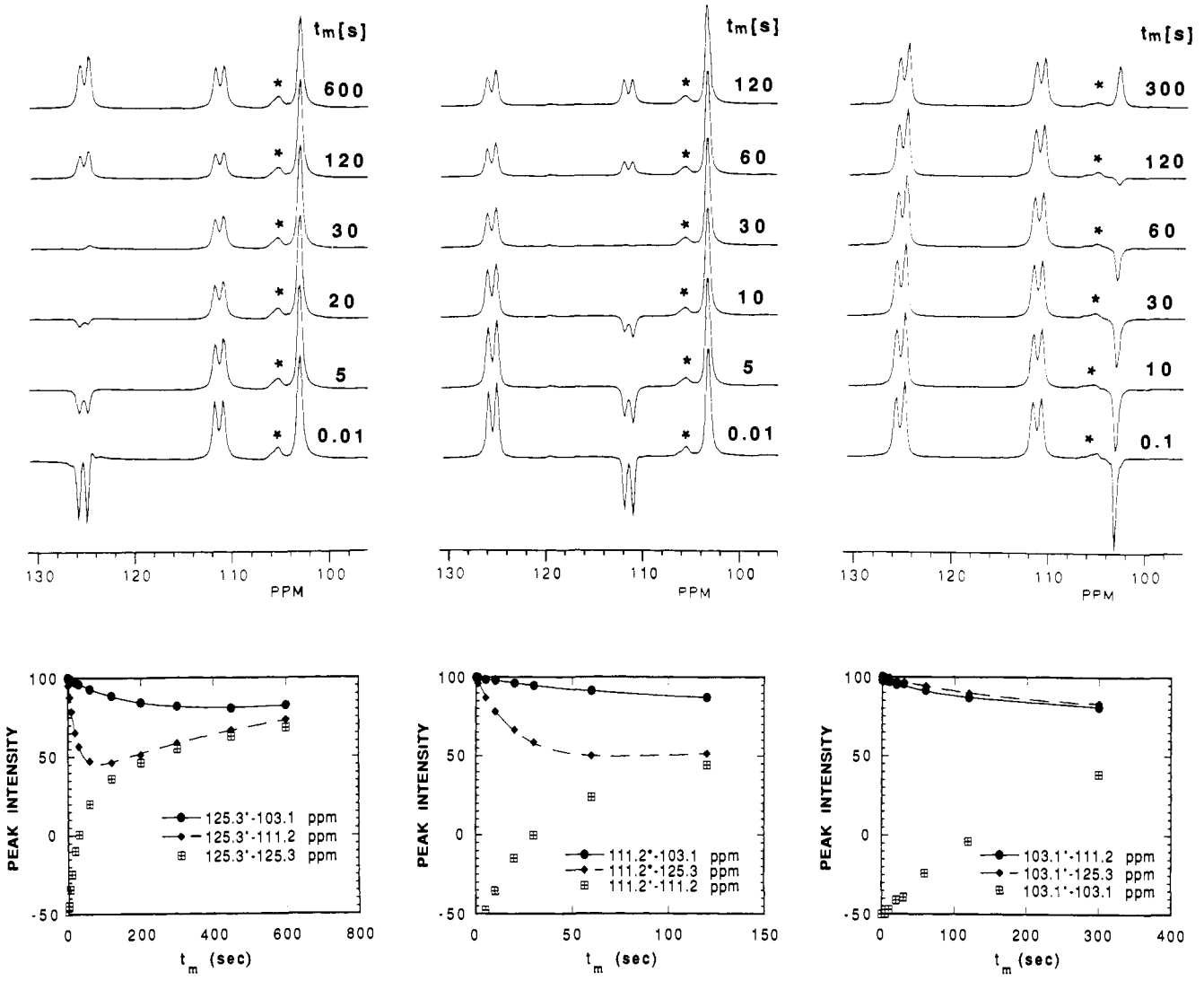

Figure 7. Spectral spin-diffusion experiments on $Ag_4P_2S_6$-II. Shown at the top of the figure are selected spectra as a function of t_m. Impurity phases that are not affected by the pulse sequence are labeled with an asterisk. The dependence of signal intensity (percent relative to the unperturbed state) on mixing time is shown at the lower part of the figure. The chemical shifts of the inverted peak (labeled with an asterisk) and of the monitored peak are indicated.

In spite of this limitation, the k values obtained give some useful qualitative insights regarding the strength of the dipole–dipole coupling. In the present application, we have used spin diffusion experiments primarily to decide whether two given resonances observed in a multipeak spectrum belong to one and the same phase or to two different phases. In the first case the cross-relaxation effects described above would be seen, whereas in the second case the intensities of the non-inverted signals would remain unaltered during the mixing period.

Discussion

Solid-State NMR Characterization of Crystalline Model Compounds in the System Ag_2S–P_2S_5. (a) $AgPS_3$. $AgPS_3$ ($x = 0.5$) is the most phosphorus rich pseudobinary compound in the system $(Ag_2S)_x$–$(P_2S_5)_{1-x}$. Crystalline compositions with higher P_2S_5 contents ($x < 0.5$) yield spectra that are quantitatively explained as mixtures of $AgPS_3$ with binary phosphorus sulfides (primarily P_4S_{10} and P_4S_9). Single-crystal X-ray studies confirm that the structure of this material is based on dimeric $P_2S_6^{2-}$ groups, corresponding to two PS_4 tetrahedra sharing a common edge.[34] The P···P distance across this edge is unusually short, corresponding to 2.89 Å. The ^{31}P MAS-NMR spectrum shows an extremely wide spinning sideband pattern, revealing a large chemical shift anisotropy (see Table II). This is understandable in view of the local phosphorus coordination, in which the wide range of S–P–S bond angles (93.7–118°) testifies to an extremely large distortion from the ideal tetrahedral geometry. Both the isotropic and anisotropic chemical shift components in $AgPS_3$ are close to those measured in crystalline $LiPS_3$, which is believed to have an analogous structure. The dipolar second moment as measured from the ^{31}P spin–echo experiment does not agree well with the value calculated from the crystal structure. Extensive model compound studies have shown that this situation can arise whenever the major contribution to the dipole–dipole coupling arises from nuclei whose difference in resonance frequencies is on the same order of (or smaller than) the dipole–dipole coupling strength.[59] In such a case, the "flip-flop" term contributes to the dipolar Hamiltonian, resulting in incomplete refocusing of chemical shift evolution by the simple Hahn–spin echo sequence. In the case of $AgPS_3$ this explanation probably accounts for the discrepancy between theory and result. The major dipolar interaction arises from the two P atoms comprising the $P_2S_6^{2-}$ units, which are both chemically and crystallographically equivalent. At each crystal orientation, the resonance frequencies of these two ^{31}P nuclei depend on the orientation of their respective chemical shift principal axis systems relative to the magnetic field direction. To make more quantitative predictions in this regard, the orientation of these tensors relative to the geometry of the $P_2S_6^{2-}$ unit must be determined from single-crystal rotation patterns.

(59) Lathrop, D.; Franke, D.; Maxwell, R.; Tepe, T.; Flesher, R.; Zhang, Z.; Eckert, H. *Solid State NMR*, in press.

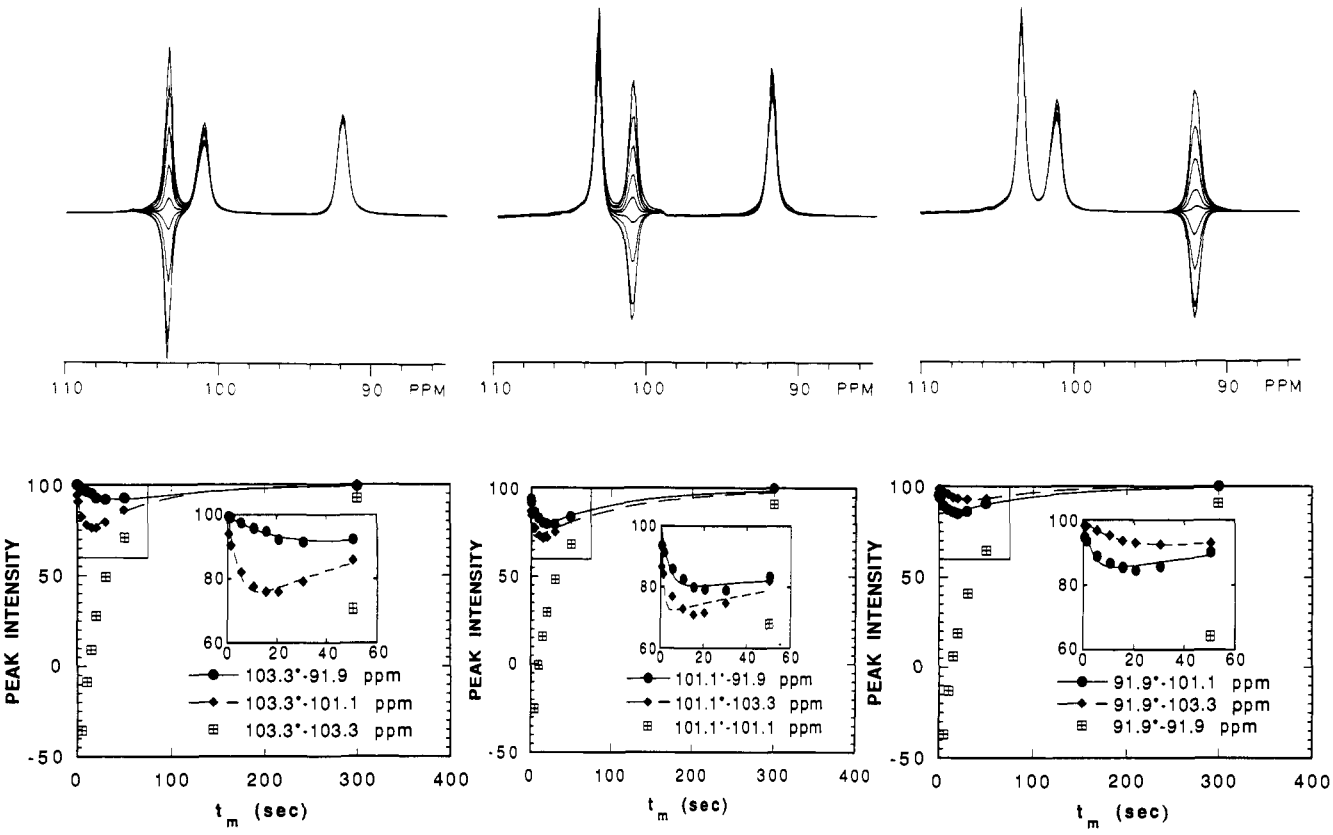

Figure 8. Spectral spin-diffusion experiments on $Ag_7P_3S_{11}$. Shown at the top of the figure is a stacked plot of the spectra over the range of t_m values used. The dependence of signal intensity (percent relative to the unperturbed state) on mixing time is shown at the lower part of the figure. The chemical shifts of the inverted peak (labeled with an asterisk) and of the monitored peak are indicated. The insets show an expanded region of the data.

(b) $Ag_4P_2S_6$-I and -II. The structures of both forms of $Ag_4P_2S_6$ are based on P–P bonded $P_2S_6^{4-}$ groups. In one of the forms synthesized at high pressure and 20% excess sulfur ("$Ag_4P_2S_6$-I") the participating P atoms are crystallographically distinct from each other. Figure 1 shows that they are separated by approximately 16 ppm on the ^{31}P NMR chemical shift scale and are split into doublets due to $^1J(^{31}P-^{31}P)$ spin–spin coupling [$^1J(^{31}P-^{31}P)$ = 109 Hz]. Figure 6 shows the result of the spin-diffusion measurement. The P–P bond is characterized by a cross-relaxation rate constant of 0.032 s^{-1}.

In the second phase ("$Ag_4P_2S_6$-II") the asymmetric unit contains two separate $P_2S_6^{4-}$ groups. The P atoms for the first group are crystallographically identical, while those of the second group are inequivalent. This situation is reflected in the solid-state NMR spectrum, which shows one singlet and two doublets. Figure 7 shows the results of a spin-diffusion measurement. Clearly, cross-relaxation occurs among all of the major spectral components, hence revealing that all of the phosphorus atoms detected in the spectrum with major intensity belong to the same crystal lattice. At the same time, spin diffusion between the doublet components is much more rapid than that between either one of the doublets and the singlet. Thus, the spin-diffusion measurements serve to distinguish very clearly between the P–P connectivity and mere spatial proximity among the two different $P_2S_6^{4-}$ groups in the crystal lattice.

(c) $Ag_4P_2S_7$. This compound shows a single peak (at 96.5 ppm), as expected from the crystal structure, which shows that both P atoms of the $P_2S_7^{4-}$ group are equivalent. The spin–lattice relaxation time of this material is extremely long (several hours). Thus, it is easy to underestimate or even miss this spectral component in experiments run with moderately long recycle delays. The second moment determined from the spin–echo experiment is in fair agreement with the value calculated from the crystal structure.

(d) $Ag_7P_3S_{11}$. The structure of $Ag_7P_3S_{11}$ contains a $P_2S_7^{4-}$ group and a PS_4^{3-} group. Accordingly, the spectrum shows three resonances at 103.3 ("a"), 101.1 ("b"), and 91.9 ppm ("c") in an approximate 1:1:1 ratio. We assign resonance "a" to the PS_4^{3-} group and the latter two to the two inequivalent P atoms of the $P_2S_7^{4-}$ group. This assignment is supported by the fact that peaks "b" and "c" have larger chemical shift anisotropies and are significantly broader than the 103.3-ppm peak. The larger anisotropies are expected due to the more distorted local geometry in the $P_2S_7^{4-}$ group,[39] whereas the broadening of the resonances is attributed to unresolved scalar spin–spin interaction between the P atoms across the sulfur bridge.

The second moment characterizing the $^{31}P-^{31}P$ dipole–dipole coupling in $Ag_7P_3S_{11}$ is in excellent agreement with the calculation from the crystal structure. The spin-diffusion measurements are shown in Figure 8. Clearly, all of the P atoms experience dipole–dipole coupling with each other, with cross-relaxation rate constants between 0.01 and 0.04 s^{-1}. This experiment confirms that all of the three resonances reflect P atoms that are part of the same crystal lattice. The differences among the three cross-relaxation rates arise from the variations in both the spatial proximity of the P atoms in the lattice and the probability of level-crossing during MAS-NMR. Thus, the relatively large spin-diffusion rate k(b–c) is explained due to the strong dipole–dipole coupling across the P–S–P bridge. On the other hand, the spin-diffusion rate constant k(a–b) is comparable to this value (in spite of a much greater internuclear distance), because the corresponding P atoms are spectrally rather close and thus presumably have a high probability of level-crossing. This latter factor is held responsible for the large difference between the cross-relaxation constants for peaks "a" and "b" and peaks "a" and "c".

(e) Ag_7PS_6 and Ag_3PS_4. Although the crystal structure of Ag_7PS_6 is not known, this compound is presumed to be a double salt, containing both PS_4^{3-} and S^{2-} groups. The ^{31}P MAS-NMR spectrum shows a sharp single resonance with very weak sidebands even at low spinning speeds, revealing a very small chemical shift anisotropy. This is expected based on the symmetry of the PS_4^{3-} group. In addition, spectra of compositions near x = 0.75 show a resonance with similar NMR characteristics at 103.0 ppm. We assign this peak to a recently reported compound of stoichiometry

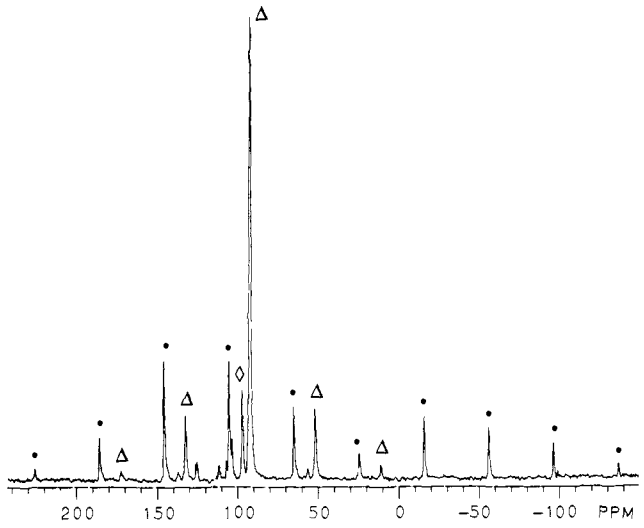

Figure 9. ^{31}P MAS-NMR spectrum of a crystallized glass with composition $x = 0.60$. Note the presence of a prominent peak at 91.5 ppm (△), in addition to crystalline $AgPS_3$, which forms the spinning sideband pattern (●). The peak marked with a ◇ represents a trace of $Ag_4P_2S_7$ (stable phase). In addition, a trace of $Ag_4P_2S_6$-II is present.

Ag_3PS_4.[40] Note that since this peak coincides with one of the resonances in $Ag_7P_3S_{11}$, the spin-diffusion experiments can be extremely valuable for peak assignments. While the NMR spectra of Ag_3PS_4 and $Ag_7P_3S_{11}$ are quite distinct, their X-ray powder patterns are strikingly similar. For this reason, this compound may have eluded detection in earlier studies.

***(f)* New Compound (Stoichiometry Uncertain).** Replicate preparations of recrystallized glasses in the composition range $0.6 \leq x \leq 0.66$ show reproducibly the appearance of new reflections in the X-ray powder pattern that cannot be reconciled with any of the stable compounds in the Ag–P–S phase field but match that reported recently for a high-temperature phase of $Ag_4P_2S_7$. The NMR spectra reveal a single resonance at 91.5 ppm in addition to the features belonging to known crystalline Ag–P–S phases. A typical spectrum of a mixture obtained at $x = 0.6$ is shown in Figure 9. The moderately small chemical shift anisotropy of the new species (see Table II) suggests that the phosphorus atoms are most likely $Q^{(1)}$ units. This assignment, which corresponds to an $x = 0.66$ stoichiometry, is also most consistent with the mass balance obtained when considering the known stoichiometries of the major impurity phases present in various preparations. The phase is absent in preparations that have been annealed for long times. Thus, all the evidence suggests that this compound is the recently reported high-temperature form[40] of $Ag_4P_2S_7$, a metastable phase that can only be preserved upon the crystallization of the glassy state.

Differentiation of Phosphorus Environments by ^{31}P NMR in Binary and Ternary Phosphorus Sulfides. The suitability of ^{31}P MAS-NMR for distinguishing between various $Q^{(n)}$ species in alkali metal phosphate glasses is well documented. Figure 10a illustrates this situation schematically for a range of crystalline silver and lithium phosphates with $Q^{(3)}$, $Q^{(2)}$, $Q^{(1)}$, and $Q^{(0)}$ sites. In contrast, the data summarized in Figure 10b clearly illustrate that in the analogous phosphorus sulfide based glasses the $Q^{(3)}$, $Q^{(2)}$, $Q^{(1)}$, and $Q^{(0)}$ species all resonate within the same identical chemical shift region. An especially wide chemical shift range (ca. 60 ppm) is seen for the $Q^{(3)}$ species (the $S = PS_{3/2}$ unit).[32] Even the P–P bonded $P_2S_6^{4-}$ groups occur within the same chemical shift region as most of the other species. The only clear assignment that can be made on the basis of isotropic chemical shift data is that to the edge-sharing dimeric $P_2S_6^{2-}$ ($Q^{(2)}$) group, which resonates distinctly upfield from the other units. Furthermore, $Q^{(2)}$ species (dimeric and polymeric) are distinguished from the other groups by a large chemical shift anisotropy, which is responsible for a wide spinning sideband pattern at typical MAS speeds (5–8 kHz). Also, from the limited range of data available,

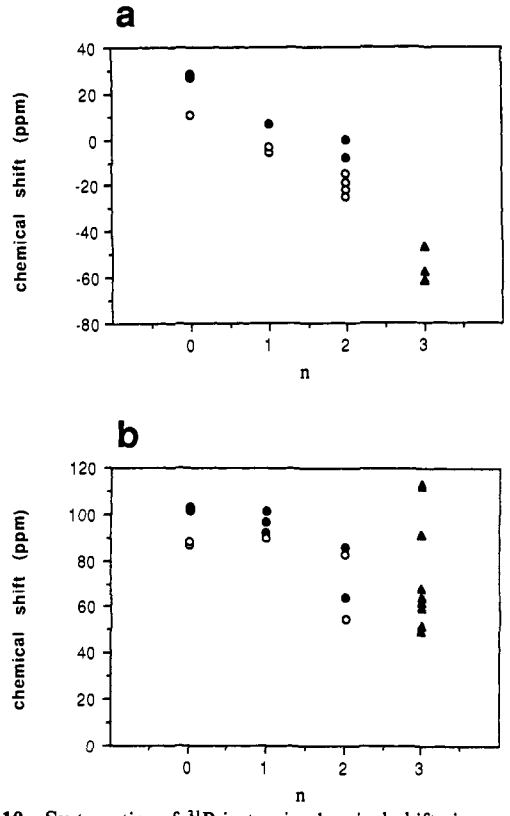

Figure 10. Systematics of ^{31}P isotropic chemical shifts in crystalline lithium and silver phosphates (open and filled circles, respectively). The chemical shift is plotted as a function of the number n, which specifies the number of P–O–P bonds in the $Q^{(n)}$ structural unit. The triangles correspond to the $Q^{(3)}$ units known to exist in various P_2O_5 polymorphs[24] (a) and binary phosphorus sulfides[32] (b).

it appears that $Q^{(1)}$ species have generally larger chemical shift anisotropies than $Q^{(0)}$ species. In this respect there seems to be a good analogy between the phosphates and thiophosphates. Another analogy that is evident from Figure 10 is the effect of the countercation. For both the oxides and the sulfides with the same $Q^{(n)}$ specification, the silver-containing phases resonate downfield of the corresponding lithium compounds, typically by ca. 10 ppm.

The lack of good chemical shift discrimination between different $Q^{(n)}$ species in thiophosphates and the dramatic upfield shift effect due to edge-sharing parallels similar observations made in the ^{29}Si MAS-NMR comparison between silicates and thiosilicates.[60]

Finally, it should be mentioned that the P–P bonded $P_2S_6^{4-}$ structure can of course be identified unambiguously by the presence of J-coupling doublets if the participating phosphorus atoms are chemically inequivalent. The spin-diffusion measurements show very rapid cross-relaxation between the directly bonded phosphorus atoms, mediated both by dipolar and scalar interactions. The spin-diffusion measurements are furthermore extremely useful for assigning crystallographically inequivalent phosphorus sites that occur within the same phase and for distinguishing those peaks from the resonances belonging to different phases. As such, these experiments are generally very useful for the spectral editing of complex multiline ^{31}P NMR spectra. This is particularly true for the present system, where there are three different compounds giving rise to a peak around 103 ppm, two compounds resonating at 91.5 and 91.9 ppm, and two compounds with chemical shifts at 101.7 and 101.1 ppm, respectively.

The model compound work also allows the assignment of specific spectral features to the $Q^{(n)}$ units present in the glasses. Due to lack of sufficient chemical shift discrimination between these units, it is, however, difficult to carry out this analysis in a quantitative fashion. Nevertheless, the NMR spectra reveal

(60) Eckert, H.; Kennedy, J. H.; Pradel, A.; Ribes, M. *J. Noncryst. Solids* **1989**, *113*, 287.

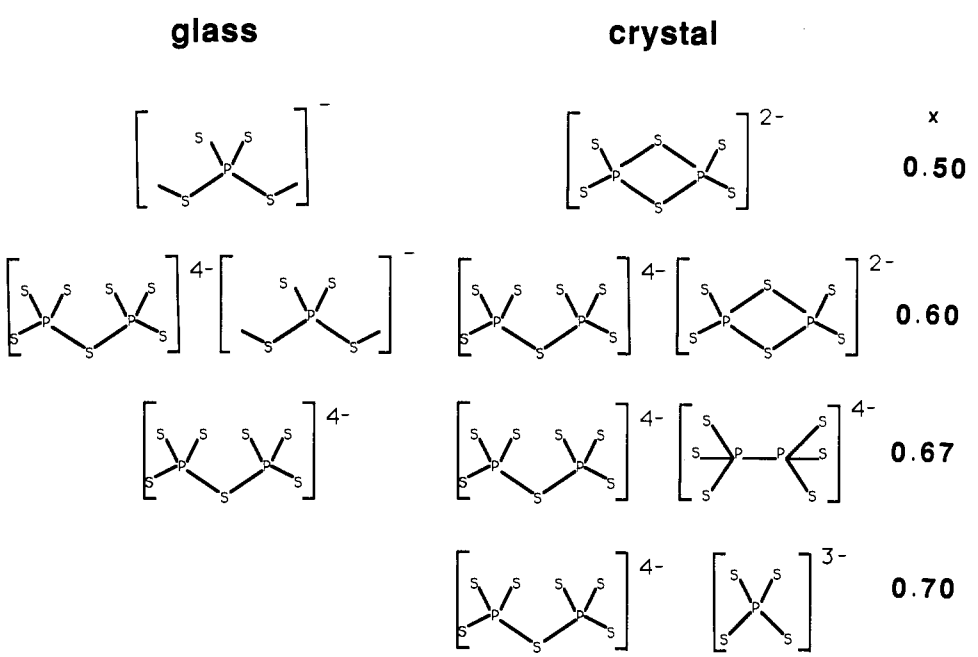

Figure 11. Structural units occurring in crystalline and glassy compositions of the system $(Ag_2S)_x(P_2S_5)_{1-x}$. The respective values of x are indicated in the figure.

a clear conceptual picture of the network structure of Ag_2S–P_2S_5 glasses as discussed below.

The Structure of Glasses in the System Ag_2S–P_2S_5. The ^{31}P MAS-NMR spectra shown in Figure 2 for pseudobinary Ag_2S–P_2S_5 glasses indicate a dramatic evolution of phosphorus short-range order as a function of composition. For $x = 0.4$ and 0.5, we observe a dominant site centered around 86–87 ppm with very intense spinning sidebands, revealing a large chemical shift anisotropy. In addition, the spectra show a shoulder around 98 ppm. As x increases beyond 0.5, this shoulder gradually becomes the dominant peak, and the 86–87-ppm feature disappears.

On the basis of the composition and the model compound work discussed above (see Table II), we assign the resonance observed in the glasses at 97–98 ppm to pyrothiophosphate ($P_2S_7^{4-}$) groups ($Q^{(1)}$ species). On the basis of composition and the large chemical shift anisotropy, the sideband pattern centered at 86–87 ppm must be assigned to a $Q^{(2)}$ species. Note, however, that the isotropic chemical shift for the dominant site in glassy $(Ag_2S)_{0.5}(P_2S_5)_{0.5}$ (nominal composition $AgPS_3$) differs by ca. 20 ppm from that measured in its crystalline counterpart. A similar chemical shift discrepancy between the glassy and the crystalline state has been observed previously for a sample with the composition $(Li_2S)_{0.5}(P_2S_5)_{0.5}$.[30] These observations can be understood by assuming that the dimeric $P_2S_6^{2-}$ groups do not exist in the glassy state in appreciable extent. Rather, the $Q^{(2)}$ units appear to form polymeric chains similar to those present in crystalline or glassy alkali metaphosphates.

The spin–echo NMR experiments are consistent with the above conclusions. Figure 4 illustrates the dependence of the dipolar ^{31}P–^{31}P second moment on composition. As expected, the second moments scale linearly with the phosphorus concentration in the glasses. The numerical values of the second moments and their compositional trend are consistent with a random distribution of the phosphorus atoms and the absence of phosphorus–phosphorus bonds within the entire glass forming region. With the exception of the composition $x = 0.5$ (stoichiometry $AgPS_3$) there is generally good agreement between the second moment in the crystalline and the glassy state. There is, however, a substantial difference in the ^{31}P–^{31}P dipole–dipole interaction strength between crystalline and glassy $AgPS_3$, again revealing the dramatic change in short-range order structure upon vitrification. The markedly reduced second moment observed in the glassy state indicates that the P···P distance of the $Q^{(2)}$ unit in the glass is much longer than that observed in the edge-shared crystalline compound.

Overall, the principles governing the structure of Ag_2S–P_2S_5 glasses (as well as their lithium analogues) are found to be quite similar to those in alkali phosphate glasses. Addition of lithium or silver sulfide to P_2S_5 introduces nonbridging sulfur atoms, resulting in a continuous network transformation. The scheme illustrated in Figure 11 summarizes the structural situation for the Ag_2S–P_2S_5 system. This scheme is generally similar but slightly more complex than that previously suggested for the Li_2S–P_2S_5 system. Contrary to the Li_2S–P_2S_5 glasses, the NMR data give no evidence for the formation of phosphorus–phosphorus bonded $P_2S_6^{4-}$ species for Ag_2S–P_2S_5 glasses. This result suggests that the $P_2S_7^{4-}$ species is more stable in the system Ag_2S–P_2S_5 compared to the lithium-containing system. The fact that crystalline $Ag_4P_2S_6$ and $Ag_4P_2S_7$ can both be synthesized while in the crystalline Li_2S–P_2S_5 system only $Li_4P_2S_6$ is stable at that composition points in the same direction.[30] The composition $x = 0.67$ marks the glass-forming border in the Ag_2S–P_2S_5 system, whereas in the lithium analogue glass formation extends to higher x values. We attribute this fact to the stability of compound $Ag_7P_3S_{11}$ (which has no lithium counterpart and acts as a thermodynamic sink toward crystallization).

Conclusions

The local structures of glasses and crystalline compounds in the system Ag_2S–P_2S_5 have been characterized by several complementary ^{31}P solid-state NMR techniques. Contrary to the situation for crystalline and glassy alkali phosphates, the phosphorus environment cannot be identified unambiguously on the basis of the ^{31}P chemical shift alone, because the chemical shift ranges for the various $Q^{(n)}$ species overlap heavily. The assignments in the crystalline state are greatly facilitated by MAS-spin-diffusion measurements.

The emerging general picture for the structure of thiophosphate glasses shows great similarity to that of alkali phosphate glasses with one important exception: Contrary to the phosphate glasses, which can be viewed as random arrangements of local environments already known in crystalline compounds, thiophosphate glasses show local environments unique to the glassy state that appear to be thermodynamically unstable in the crystalline form. The opportunity of "trapping" such species in the glassy state appears to be a not uncommon feature of non-oxide chalcogenide glasses[60,61] and illustrates their significance in structural chemistry.

Acknowledgment. We thank Dr. James P. Yesinowski (Naval

(61) Pradel, A.; Michel-Lledos, V.; Ribes, M.; Eckert, H. *Solid State Ionics* **1992**, in press.

Research Laboratory) for directing our attention toward the spectral spin-diffusion experiment, for a preprint of his manuscript, and for helpful discussions. Thanks are also due to Drs. David Lathrop and Regina Francisco and to Ms. Deanna Franke for help with the data analysis. Acknowledgment is made to the donors of the Petroleum Research Fund, administered by the American Chemical Society, and to the National Science Foundation (Grant DMR 89-13738) for financial support of this research.

Molecular Orbital Studies of the Structure and Reactivity of Model Substrate Intermediates in the Deacylation of the Cysteine Protease Papain

Gregory D. Duncan,[†,‡] Carol P. Huber,[§] and William J. Welsh*[,†]

Contribution from the Department of Chemistry, University of Missouri—St. Louis, St. Louis, Missouri 63121, and National Research Council of Canada, Ottawa, Ontario, Canada K1A OR6.
Received September 18, 1989

Abstract: Molecular orbital calculations suggest that an interaction between the substrate amide nitrogen of substituted *N*-benzoylglycine (dithioacyl) papains and the thiol sulfur of cysteine-25 is not only catalytically important, it is part of the catalytic mechanism. AM1 indicates that, during hydrolysis of the dithio ester intermediate, charge is exchanged via orbital interactions and in particular between the HOMOs associated with the reaction site and the LUMOs associated with the benzamide portion of the substrate. Charge delocalization emanating from this effect stabilizes the anionic tetrahedral intermediate formed during deacylation, thereby lowering its activation energy and providing the catalytic effect. The unexpected strong effect of electron-withdrawing and -donating groups (located on the substrate's benzamide phenyl) on deacylation kinetics is explained in terms of their ability to promote or inhibit this charge delocalization. The present computational results together with previous spectroscopic studies suggest that the enzyme specifically promotes this interaction in its binding of the substrate. The relative reactivities of dithio esters and thiol esters are contrasted in terms of their electronic features. Both AM1 and ab initio results indicate a reversal of bond polarity for the C=S bond in the dithio ester moiety [C(=S)—S] relative to the C=O bond in the thiol ester moiety [C(=O)—S]. The approximately 20-fold higher rate of deacylation for the thiol ester relative to the dithio ester may in part be accounted for by the increased stability of the tetrahedral intermediate for the dithio ester relative to the thiol ester.

Introduction

The cysteine proteases comprise a group of proteolytic enzymes which depend on the reactive thiol group (-SH) of a cysteine residue (Cys-25 in papain) for their enzymatic activity. Like the analogous serine proteases, they serve a variety of biological functions although the precise role of many of them remains unknown. The cysteine proteases are widely distributed in nature, including the cathepsins B, H, and L in mammalian tissues, the plant enzymes papain, ficin, bromelain, and actinidin, and the bacterial cysteine proteases clostripain (from *Clostridium histolyticum*) and streptococcal proteinase (from hemolytic streptococci).[1-4]

The crystal structure of papain has been determined at high resolution by X-ray crystallography.[2] Likewise, its binding-site region and proposed mechanism of action have been characterized on the basis of the observed binding of substrate analogues.[2,3] The enzyme is described as being composed of two domains separated by a cleft which contains the active site (Figure 1).[1-4] The binding site for the substrate straddles this cleft with Cys-25 and His-159 located in close proximity but on opposite sides of the cleft. By virtue of its well-positioned imidazole ring [Im], His-159 is believed to act as a general-base catalyst. This might be achieved by forming an ion pair [RS^-·HIm^+] with the thiol group of Cys-25, thereby activating the latter's nucleophilicity.

The reaction pathway for the papain-catalyzed hydrolysis of substrates (Figure 2) can be represented simply as binding, after which the enzyme is first acylated (Figure 2, steps b–d) then deacylated (Figure 2, steps e–f). The overall kinetics of acylation and deacylation is quantified in terms of the specific rate constants k_2 and k_3, respectively. The rate-determining step at both acylation and deacylation is purported to involve formation and subsequent breakdown of a transient anionic tetrahedral intermediate.

The focus of the present study is the catalytic mechanism of the deacylation reaction in papain as a representative cysteine protease. The acylation step, which immediately precedes deacylation, is responsible for the cleavage of peptide bonds in protein substrates. This cleavage yields an intermediate in which the acyl terminal portion of the cleaved substrate forms a bond with the sulfur atom of Cys-25. The intermediate so formed is a thiol ester [C- (=O)—S] in the biological system. As with many other proteases, papain also cleaves ester substrates. Once again, the intermediate formed contains a thiol ester linkage. However, if a thiono ester [C(=S)—O] substrate is used instead of an ester [C(=O)—O] substrate, the resulting linkage is a dithio ester [C(=S)—S]. A minimal reaction scheme for these two possibilities is illustrated in Figure 3.

Certainly, the dithio ester linkage is not indigenous to the biochemistry of cysteine proteases. Yet its unique structural

* Author to whom inquiries should be addressed.
† University of Missouri—St. Louis.
‡ National Research Council of Canada.
‖ Present address: Department of Chemistry, University of Southern California, Los Angeles, CA 90089.

(1) Polgar, L.; Halasz, P. *Biochem. J.* **1982**, *207*, 1. Willenbrock, F.; Kowlessur, D.; O'Driscoll, M.; Patel, G.; Quenby, S.; Templeton, W.; Thomas, E. W.; Willenbrock, F. *Biochem. J.* **1987**, *244*, 173. Asboth, B.; Polgar, L. *Biochemistry* **1983**, *22*, 117. Polgar, L.; Asboth, B. *Proc. FEBS Congr., 16th* (Moscow, June 1984) **1985**, *A*, 17. Willenbrock, F.; Brocklehurst, K. *Biochem. J.* **1985**, *227*, 521.
(2) Kamphuis, G.; Kalk, K. H.; Swarte, B. A.; Drenth, J. *J. Mol. Biol.* **1984**, *179*, 233.
(3) Drenth, J.; Kalk, K. H.; Swen, H. M. *Biochemistry* **1976**, *15*, 3731.
(4) (a) Lowe, G. *Tetrahedron* **1976**, *32*, 291. (b) Fersht, A. *Enzyme Structure and Function*, 2nd ed.; W. H. Freeman and Co.: New York, 1985; p 415.

0002-7863/92/1514-5784$03.00/0